cycling. Details of impedance and long-term cycling behavior of $Li_4Ti_5O_{12}/LiMn_2O_4$ cells are presented elsewhere.[13]

Energy densities of cells.—The estimated specific energies of the Li/PAN electrolyte/$Li_4Ti_5O_{12}$ and $Li_4Ti_5O_{12}$/PAN electrolyte/$LiMn_2O_4$ cells when fully packaged are 57 and 60 Wh/kg, respectively. The load voltages of 1.5 and 2.6 V, respectively, were used in the calculation along with the actual weights and capacities of the electrodes, and the weights of the polymer electrolyte membrane and the current collectors. The specific energies may limit the widespread use of these cells; but they may be of interest for special applications where specific energy is less of a concern than long cylce life.

Acknowledgment

This work was carried out on contract DE-FG02-96ER82158 from the U.S. Department of Energy.

Manuscript submitted August 21, 1997; revised manuscript received March 19, 1998.

REFERENCES

1. T. Ohzuku, A. Ueda, and N. Yamamoto, *J. Electrochem. Soc.*, **142,** 1431 (1995).
2. T. Ohzuku, A. Ueda, N. Yamamoto, and Y. Iwakoshi, *J. Power Sources,* **54,** 99 (1995).
3. K. M. Kolbow, J. R. Dahn, and R. R. Haering, *J. Power Sources,* **26,** 397 (1989).
4. E. Ferg, R. J. Gummow, A. de Kock, and M. M. Thackeray, *J. Electrochem. Soc.,* **141,** L147 (1994).
5. K. M. Abraham, D. M. Pasquariello, T. H. Nguyen, Z. Jiang, and D. Peramunage, in *Proceedings of the Annual Battery Conference, IEEE Aerospace and Electronic System Society,* IEEE (1996).
6. T. Ohzuku, M. Kitagawa, and T. Hirai, *J. Electrochem. Soc.,* **137,** 769 (1990).
7. J. M. Tarascon, E. Wang, F. K. Shokoohi, W. R. McKinnon, and S. Colson, *J. Electrochem. Soc.,* **138,** 2859 (1991).
8. Z. Jiang and K. M. Abraham, *J. Electrochem. Soc.,* **143,** 1591 (1996).
9. H. S. Choe, B. G. Carroll, D. M. Pasquariello, and K. M. Abraham, *Chem. Mater.,* **9,** 369 (1997).
10. K. M. Abraham and M. Alamgir, *J. Power Sources,* **43-44,** 195 (1993).
11. E. Peled, *J. Electrochem. Soc.,* **126,** 2047 (1979).
12. D. Aurbach and Y. Gofer, *J. Electrochem. Soc.,* **136,** 3198 (1989).
13. D. Peramunage and K. M. Abraham, *J. Electrochem. Soc.,* **145,** 2615 (1998).

The $Li_4Ti_5O_{12}$//PAN Electrolyte//$LiMn_2O_4$ Rechargeable Battery with Passivation-Free Electrodes

D. Peramunage* and K. M. Abraham*,[a]

EIC Laboratories, Incorporated, Norwood, Massachusetts 02062, USA

ABSTRACT

The Li-ion cell, $Li_4Ti_5O_{12}$//PAN electrolyte//$LiMn_2O_4$, appears to be a classic example of a battery with passivation-free electrodes. Its gross impedance characteristics remain steady during long-term cycling at high charge/discharge rates. The cell showed excellent rechargeability at >99.9% coulombic efficiency for nearly 250 full-depth cycles, at a 1C discharge rate and a C/5 charge rate. The capacity fade was low at approximately 0.12% per cycle at around 100 cycles and ~0.05% at around 200 cycles. Excellent utilizations of the cathode and anode were observed with values of 100 mAh/g of $LiMn_2O_4$ and 140 mAh/g of $Li_4Ti_5O_{12}$ at 1C discharge rate, and 70 mAh/g of $LiMn_2O_4$ and 92 mAh/g of $Li_4Ti_5O_{12}$ at 7.5C discharge rate. Electrode utilizations were significantly better under pulse discharge conditions at the 8C-16C rates. The energy density of the cell, calculated with a cell voltage of 2.6 V and practically observed cathode and anode capacities at the C/10 discharge rate, is 60 Wh/kg. The weights of the electrodes, current collectors, and electrolyte are included in this value. It is suitable for applications where high power and very long cycle life are required.

Introduction

High power batteries are becoming increasingly important for powering modern consumer products such as cellular telephones, portable power tools, laptop computers, video cameras, and electric vehicles. Discharges at rates as high as the 5C rate are required for some of these applications. The power of a battery, P, is related to its operating voltage, V, and the current, I, according to the relationship

$$P = V I \quad [1]$$

Operating voltage can be expressed in terms of a number of parameters related to the materials, design, and operation of a battery[1]

$$V = (U^\circ - \eta^{a,c} - \phi^{a,c} - \phi_{pf}^{a,c} - \phi_{el} - \phi_\Omega^{a,c}) \quad [2]$$

Where U° is the emf of the cell in volts, $\eta^{a,c}$ are the surface overpotentials at the anode, and the cathode related to their charge-transfer resistances, $\phi^{a,c}$, $\phi_{pf}^{a,c}$, ϕ_{el}, and $\phi_\Omega^{a,c}$ are the potential drops due to concentration polarization, passivation layers on both electrodes, the electrolyte, and contact resistance, respectively. EMF of the cell, U°, is fixed by the type of active materials used for the anode and the cathode, and, ideally, it represents the maximum operating voltage possible for a given system. Since the potential drops included in Eq. 2 make the actual operating voltage smaller than this ideal maximum, minimizing them is necessary to ensure the highest power output. Accordingly, low ϕ_{el} with the use of a thin, highly conductive, electrolyte layer and low $\eta^{a,c}$ by means of electrodes with fast Li insertion kinetics are desirable. At high discharge rates, concentration polarization, $\phi^{a,c}$, resulting from diffusion limitations of Li^+ in the solid cathode (anode) and the electrolyte phases becomes a relevant issue. Such difficulties could be circumvented by minimizing the time constant for Li^+ diffusion in the solid-state, L^2/D (L = diffusion width in centimeters, and D is the diffusion coefficient in centimeters squared per second),[2] using smaller size particles (meaning smaller L). Diffusion problems arising in the electrolyte, especially the electrolyte phase included in the bulk of the composite electrode can be controlled by using thinner electrodes.[3,4] In order to minimize the potential drop due to contact resistance, $\phi_\Omega^{a,c}$, within a composite electrode, high surface-area carbon is usually included as a conductivity enhancing additive. In general, proper electrode engineering appears to be a key factor in minimizing the contact resistance.

* Electrochemical Society Active Member.
[a] Present address: Covalent Associates, Inc., Woburn, MA 01801, USA.

Since Li is thermodynamically incompatible with organic electrolytes, reactions occur as soon as it comes in contact with them, and the surface of Li gets immediately covered with a coating of the reaction products. Passive film formation is also possible with Li intercalated carbons (LiC_6) such as the carbon anode of a Li-ion cell. In either case, passivation layers at the anode/electrolyte interface present a major source of the potential drop, ϕ_{pf}. These layers usually continue to grow, albeit at low rates, on these anode surfaces as the cell is repeatedly charged and discharged with the result that the potential drop inside the passivation layers increases during the lifetime of a Li or Li-ion battery. When ϕ_{pf} becomes too large, the battery usually fails. Understanding the nature of the chemical reactions that lead to passive film formation on the anode surface and controlling them have been the subject of many investigations.[5-10] Recently, we have shown that the passive film that forms on a carbon anode during Li intercalation in cells containing the polyacrylonitrile (PAN)-ethylene carbonate (EC)-propylene carbonate (PC)-$LiPF_6$ solid polymer electrolyte is primarily Li_2CO_3.[10,11] It is formed according to

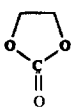

$$+ 2e^- + 2Li^+ \rightarrow Li_2CO_3 + CH_2{=}CH_2 \quad [3]$$

EC

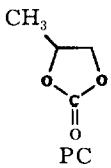

$$+ 2e^- + 2Li^+ \rightarrow Li_2CO_3 + CH_3CH{=}CH_2 \quad [4]$$

PC

The reactions shown in Eq. 3 and 4 will occur when the carbon anode potential is at or below about 1 V vs. Li^+/Li. Therefore, a Li-ion cell based on an anode that intercalates Li at potentials higher than 1 V vs. Li^+/Li will be free of passivation layers on the anode and, ϕ_{pf}, should not be a factor determining its performance. The Li-ion cell, $Li_4Ti_5O_{12}$//polymer electrolyte//$LiMn_2O_4$, reported in this paper is a classic example of such a system. Development and evaluation of its individual electrodes are presented elsewhere.[12] The electrochemical behavior of $Li_4Ti_5O_{12}$ in Li cells with organic liquid electrolytes has been reported previously.[13,14]

Experimental

Synthesis of $Li_4Ti_5O_{12}$, $LiMn_2O_4$, fabrication of individual composite electrodes and their electrochemical characterization were carried out as described in the previous paper.[12]

The PAN electrolyte of the composition 21 mole percent (mol %) PAN:36.5 mol % EC:36.5 mol % PC:6 mol % $LiPF_6$ was prepared as described previously.[10,12,15] The electrolyte had a conductivity of $\sim 2 \times 10^{-3}\ \Omega^{-1}\ cm^{-1}$ and a thickness of about 80 μm.

Fabrication of $Li_4Ti_5O_{12}$//PAN-polymer electrolyte//$LiMn_2O_4$ cells.—The cell was prepared by sandwiching the solid polymer electrolyte between a $Li_4Ti_5O_{12}$ composite anode and a $LiMn_2O_4$ composite cathode, packaging the cell in a metallized plastic envelope, evacuating and heat-sealing the envelope at the edges. Electrode preparation, cell construction, and sealing were done in an Ar-filled glove box. The compositions of the composite electrodes are given in the figure captions. The theoretical $Li_4Ti_5O_{12}$ capacity is based on three Li per formula unit and the theoretical capacity of $LiMn_2O_4$ is based on one Li per formula unit. The cell contained a Li reference electrode also. A computer controlled Arbin battery cycler was used for cycle testing at constant currents.

Impedance measurement of composite electrodes.—The experimental setup consisted of an EG&G PAR (model 273) potentiostat/galvanostat and EG&G lock-in analyzer (model 5208) in the frequency range of 0.1 Hz to 100 kHz to apply a 5 mV ac modulation across the Li-ion cell under open-circuit condition. Five points per decade were measured. The impedance data were plotted as a function of frequency in a complex plane diagram (Cole-Cole plot).

Equilibrium potential measurement.—Open-circuit voltage measurements as a function of state of charge were done during the course of a full charge/discharge cycle between potential limits from 2.9 to 1.2 V. Charge or discharge was done in steps, with the application of a series of short current steps and long rest periods in an alternative fashion, until the cutoff voltage was reached. During charge, a 0.1 mA/cm^2 (~C/5 rate) current step of 500 s was followed by a 4000 s rest period and during discharge, 0.5 mA/cm^2 (~C rate) current steps of 100 s and rest periods of 4000 s were used.

Pulsed power measurement.—The pulsed power performance of $Li_4Ti_5O_{12}/LiMn_2O_4$ battery cells were tested by first charging the cell at 0.02 mA/cm^2 to 2.9 V, and then pulse discharging to 1.2 V. The setup used for the pulse experiment consisted of an EG&G PAR 363 potentiostat/galvanostat controlled by a computer using a program based on the ASYST data acquisition system which was developed in-house. The program allowed the cell to be continuously pulse-discharged using a sequence of fast current steps of short duration with interpulse rest periods between them. Typically, the pulse lasted for 10 ms and the rest period for 50 ms. The cell voltage during the time the current is applied (ON voltage) and when it is turned off (OFF voltage) is collected by the computer over the entire pulse sequence. The pulse sequence ended whenever the load voltage reached the preset lower cell voltage limit. Complete voltage description of individual pulses could be recovered by using a Bascom-Turner BT5000 fast data acquisition system connected to the voltage signal output terminal of an EG&G PAR 363.

Results and Discussion

Cycle performance of $Li_4Ti_5O_{12}$//solid polymer electrolyte//$LiMn_2O_4$ Cells.—We have determined the charge/discharge characteristics of $Li_4Ti_5O_{12}$ and $LiMn_2O_4$ individually as described in the previous study.[12] These characteristics include: (*i*) the cathode can be charged and discharged up to a capacity of 0.8 Li per $LiMn_2O_4$, (*ii*) the $Li_4Ti_5O_{12}$ anode can be discharged and charged 2.7 Li per $Li_4Ti_5O_{12}$ or 163 mAh/g. These data serve as a guide to match capacities of the two electrodes that constitute a Li-ion cell. The individual electrode reactions and the overall cell reaction in the cell are

Anode

$$Li_4Ti_5O_{12} + 2.7Li^+ + 2.7e^- \underset{\text{Discharge}}{\overset{\text{Charge}}{\rightleftharpoons}} Li_{6.7}Ti_5O_{12} \quad [5]$$

Cathode

$$3.4LiMn_2O_4 \underset{\text{Discharge}}{\overset{\text{Charge}}{\rightleftharpoons}} 3.4Li_{0.2}Mn_2O_4 + 2.7Li^+ + 2.7e^- \quad [6]$$

Cell

$$Li_4Ti_5O_{12} + 3.4LiMn_2O_4 \underset{\text{Discharge}}{\overset{\text{Charge}}{\rightleftharpoons}} Li_{6.7}Ti_5O_{12} + 3.4Li_{0.2}Mn_2O_4 \quad [7]$$

In practice, however, the ratio of the two capacities are maintained in such a way that the cell configuration becomes slightly cathode limited. Selected capacity vs. voltage profiles for the $Li_4Ti_5O_{12}/LiMn_2O_4$ cell are presented in Fig. 1. The cell was charged at 0.12 mA/cm^2 (C/5) and discharged at 0.6 mA/cm^2 (~C) and cycling was done between upper and lower limits of 2.9 and 1.2 V, respectively.

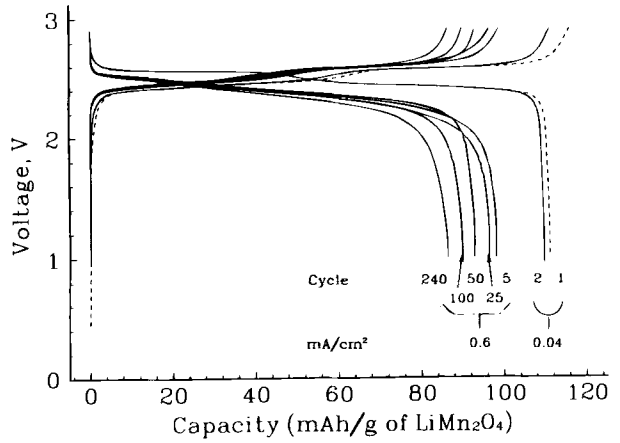

Fig. 1. Selected cycling curves at room temperature for a $Li_4Ti_5O_{12}$//solid polymer electrolyte//$LiMn_2O_4$ cell. The cathode was 85.0 wt % $LiMn_2O_4$:10.0 wt % Chevron C:2.5 wt % PVdF:2.5 wt % PAN soaked with $LiAsF_6$-containing electrolyte, had 4.73 mAh capacity, 10 cm² (2.5 × 4.0 cm) active area and a thickness of 45 μm. The anode was 87.5 wt % $Li_4Ti_5O_{12}$:10.0 wt % Chevron C:2.5 wt % PAN soaked with $LiPF_6$-containing electrolyte, had 4.77 mAh capacity, 11.3 cm² (2.7 × 4.2 cm) active area, and a thickness of 30 μm. The solid polymer electrolyte was 21.0 mol % PAN:36.5 mol % EC:36.5 mol % PC:6.0 mol % $LiPF_6$ and a thickness of 88 μm. Current density used during cycling is indicated.

Capacity vs. cycle number.—Capacity as a function of cycle life for the same cell is presented in Fig. 2. Stability of the capacity was checked intermittently by lowering the discharge rate to 0.12 mA/cm² (C/5). Slightly diminishing capacity observed during stability checks suggests that the capacity loss is real and, most likely, of materials origin and not related to any polarization phenomenon occurring at high rate. Since Li/$Li_4Ti_5O_{12}$ cells cycles with practically no capacity fade,[12] the fade observed in the full cell may be related to $LiMn_2O_4$.

Equilibrium potential measurement.—The open-circuit potential of a $Li_4Ti_5O_{12}$//solid polymer electrolyte// $LiMn_2O_4$ cell was monitored as a function of its depth of charge and discharge during the course of a full charge/discharge cycle. Evolution of the equilibrium and load potentials as a function of capacity are depicted in Fig. 3. Despite the differences in charge and discharge rates, the equilibrium potential during charge and discharge matched up with no significant hysteresis confirming that the Li insertion and deinsertion processes at both electrodes are perfectly reversible. The excellent reversibility of the system is further demonstrated by the long-term cycling data discussed above.

Impedance vs. cycle number and the demonstration of passivation free electrodes.—Impedance spectrum of a $Li_4Ti_5O_{12}$//solid polymer electrolyte//$LiMn_2O_4$ cell was taken intermittently during long-term cycling at a 0.12 mA/cm² (C/5) charge rate and a 0.6 mA/cm² (~C) discharge rate. The measurement was done at the open-circuit potential following a full discharge. Depicted in Fig. 4a and b are the Cole-Cole impedance plots measured in the three- and two-electrode configurations, respectively, at the second and 227th cycles. The working electrode is $LiMn_2O_4$. A number of distinct features are immediately visible: (*i*) a fully resolved single semicircle displaced along the Z' axis is present in the high frequency domain; (*ii*) the low frequency domain of the spectrum taken at cycle two consists of features resembling a combination of more than one semicircle whereas the corresponding region of the spectrum for cycle 227 appears to have just one semicircle; and (*iii*) the impedance response of the cell remained steady through the long-term cycling process.

Impedance measurements have been frequently used to study passivation film formation at the Li/organic electrolyte interface.[16-18] Some studies have also dealt with the insertion of Li into host materials.[19,20] In the absence of any surface layers, the impedance of an insertion electrode can be interpreted in terms of a simple network consisting of the bulk electrolyte resistance, R_e, in series with a RC network made of two parallel current branches; (*i*) a faradaic-current branch represented by a charge-transfer resistance, R_{ct}, serially connected to a Warburg impedance, Z_w, and (*ii*) a nonfaradaic-branch consisting of the double-layer capacitance, C_{dl}. The corresponding equivalent circuit consists of a single semicircle touching down at the Z axis at R_b on the high frequency side and at $R_b + R_{ct}$ on the low frequency side. The semicircle also has a spur at the low frequency side (at approximately 45° angle on the right) due to Warburg resistance, Z_w, characteristics of a diffusion process. The spectra shown in Fig. 4 consist of an isolated semicircle anticipated for $R_{ct}C_{dl}$ coupling, but instead of a straight line (spur), the low frequency end of this semicircle is connected to one or more semicircles. Such behavior in the Li/$LiCoO_2$ cell has been attributed to the presence of a thin surface film at the $LiCoO_2$/organic electrolyte interface[19] resulting from a chemical reaction between $LiCoO_2$ and the organic electrolyte. Although no account of such film formation on $LiMn_2O_4$ has been reported in prior studies, electrolyte oxidation is believed to occur on the surface of $LiMn_2O_4$.[21,22] However, long-term cycling of $Li_4Ti_5O_{12}$//solid polymer electrolyte//$Li_xMn_2O_4$ cells proceeded with almost 100% coulombic efficiency and, consequently, the amount of $Li_xMn_2O_4$ involved in a parasitic surface film formation appears to be extremely

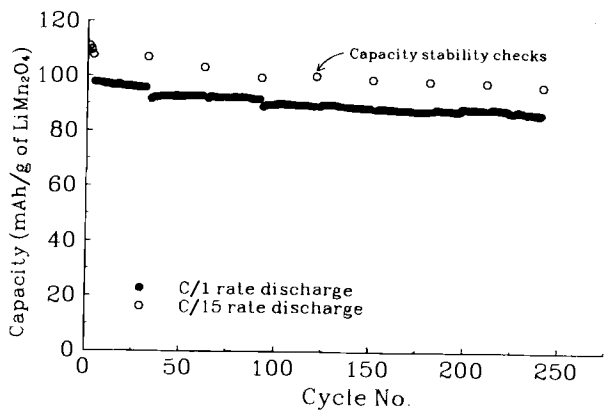

Fig. 2. Capacity vs. cycles for the cell shown in Fig. 1. The cell was charged at 0.12 mA/cm² (C/5) and discharged at 0.6 mA/cm² (~1C). Discharge rate of 0.12 mA/cm² (C/5) used during stability checks, indicated by the points.

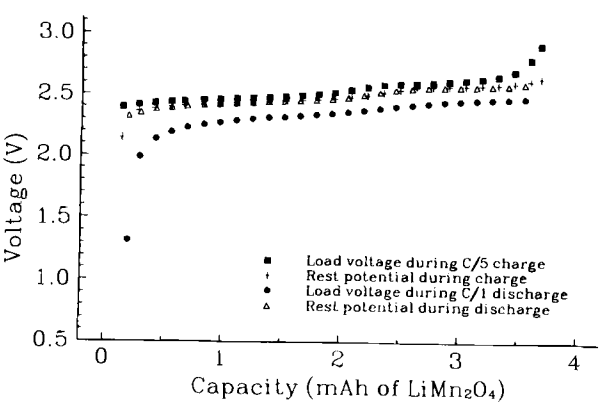

Fig. 3. The intermittent charge/discharge curves and the corresponding open-circuit voltages of a $Li_4Ti_5O_{12}$//solid polymer electrolyte//$LiMn_2O_4$ cell.

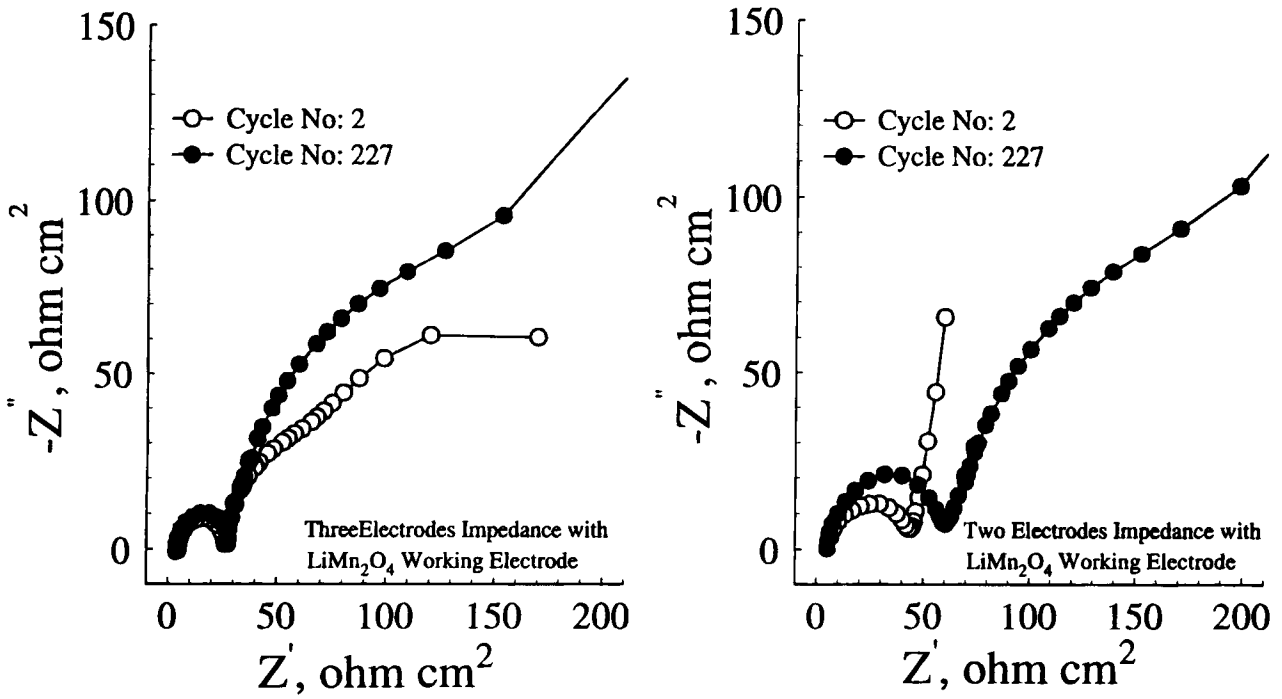

Fig. 4. Impedance response of a typical $Li_4Ti_5O_{12}$//solid polymer electrolyte//$Li_xMn_2O_4$ cell in cycles 2 and 227. (a, left) Impedance response of a typical $Li_4Ti_5O_{12}$//solid polymer electrolyte//$LiMn_2O_4$ cell in cycle 2 and 227 measured in three-electrode configuration with $LiMn_2O_4$ as the working electrode. (b, right) Impedance measured as in Fig. 4a except in two-electrode configuration with $LiMn_2O_4$ as the working electrode.

small. An interface with a surface layer can be modeled by adding another $R_{sl}C_{sl}$ component (where "sl" stands for surface layer) to the original $R_{ct}C_{dl}$ network, as shown in Fig. 5.[19]

The semicircle due to $R_{sl}C_{sl}$ coupling is located at lower frequencies compared to the frequency domain where $R_{ct}C_{dl}$ coupling occurs. The frequency corresponding to the top of a semicircle, F_{top}, is related to the RC components of the corresponding network by $f_{top} = 1/(2\pi RC)$ and the capacitance, C, is related to the thickness l by $C = \epsilon(A/l)$ where ϵ is the permitivity and A is the interfacial area. Since f_{top} of the semicircle for $R_{sl}C_{sl}$ coupling is smaller than that for $R_{ct}C_{dl}$ coupling, $R_{sl}C_{sl} >> R_{ct}C_{dl}$. Moreover, if R_{sl} is only a few times larger than R_{ct} as it appears in Fig. 4, C_{sl} should be higher than C_{dl} as expected for a thin surface layer. This study was not extended to include a detailed analysis of either the impedance data or to determine the nature of these surface layers. What is significant is the fact that the interfacial behavior remains steady during the long-term cycling of the $Li_4Ti_5O_{12}$//solid polymer electrolyte//$LiMn_2O_4$ full cell. No significant passivation other than the thin surface layer formed initially at the solid cathode/electrolyte interface is evident and the cell remained essentially passivation-free during extended full-depth cycling at high rates. The R_b and R_{ct} values were determined graphically from the impedance spectra and tabulated as a function of cycle number in Table I.

Impedance measurement across the cell (two electrode impedance) involves the combined effect of the individual networks representing the faradaic and nonfaradaic processes occurring at each electrode. In the three-electrode configuration, impedance response is mostly that of the working electrode plus a minor contribution from the electrolyte. The data in Table I and Fig. 4a and b suggest that R_b and R_{ct} values of the cathode remains steady during the course of the extended cycling while those of the anode appears to show a moderate increase. In other words, there is little change in the overall impedance of each electrode during the extended cycling.

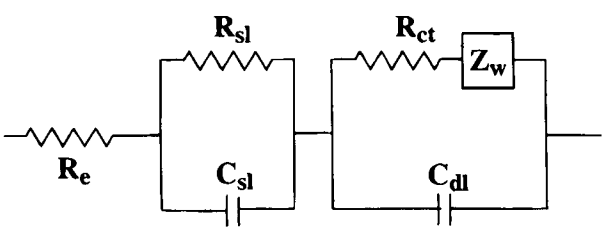

Fig. 5. Proposed equivalent circuit corresponding to the impedance spectra in Fig. 4. R_e is the bulk electrolyte resistance; R_{ct}, the charge-transfer resistance; R_{sl}, the surface layer resistance; C_{dl}, the double-layer capacitance; and Z_w, the Warburg Impedance.

Rate capability of $Li_4Ti_5O_{12}$//solid polymer electrolyte// $LiMn_2O_4$ cells.—Although the electrodes in all our Li_4/Ti_5O_{12}//solid polymer electrolyte//$LiMn_2O_4$ cells were fabricated and processed alike, for reasons unclear to us some cells showed an initial impedance (in the three-electrode configuration) much higher than the ~40 Ω cm² we normally observed. Rate capability of such a cell can be compared to that of a normal cell to demonstrate the detrimental effect of high overall impedance on the rate capability.

Rate capabilities of two Li_4/Ti_5O_{12}//solid polymer electrolyte//$LiMn_2O_4$ cells, A (DP022-50) and B (DP022-55), are presented in Fig. 6 and 7, respectively, for discharge rates ranging from 0.02 to 5 mA/cm² while maintaining a constant charge rate of 0.02 mA/cm². Both cells show comparable utilization up to a discharge rate of 1C which is about 100 mAh/g or 0.68 Li per $LiMn_2O_4$. At higher rates, however, utilization of cell A (Fig. 6) with the higher overall impedance lags considerably behind that of cell B (Fig. 7).

Impedance spectra of these two cells measured after two cycles are presented in Fig. 8. The bulk impedance, R_b, of both cells in Fig. 8 remained close to 6 Ω cm². Charge transfer impedance of cell A (DP022-50) appears to be on the order of 100 Ω cm² (Fig. 8a) while that of cell B (DP022-55) remains at ~40 Ω cm² (Fig. 8b). Since impedance spectra of each cell in the two- and three-electrode configurations exhibit similar R_b and R_{ct} values and since

Table I. Impedance data of the $Li_4Ti_5O_{12}$//solid polymer electrolyte//$LiMn_2O_4$ full cell during long-term cycling.

Cycle No.	Three-electrode impedance with $LiMn_2O_4$ working electrode and Li reference		Two-electrode impedance with $LiMn_2O_4$ working electrode	
	R_b (Ω cm^2)	R_{ct} (Ω cm^2)	R_b (Ω cm^2)	R_{ct} (Ω cm^2)
Prior to cycling	5	25	-	-
2	5	26	-	46
27	5	30	-	-
52	5	32	-	-
77	5	35	-	-
102	4	28	5	53
127	4	27	-	-
152	4	27	-	-
177	4	27	5	60
202	4	27	5	62
227	4	28	5	65

$LiMn_2O_4$ is the working electrode, the higher impedance of cell A is coming predominantly from the cathode. Apart from the differences in the R_{ct}, the two impedance spectra are different in the low frequency domain where contributions from the Warburg diffusional impedance predominate. The data to be discussed below show that the polarization of the anode is similar in both cases implying that the porous cathode structure is the factor responsible for the difference between cells A and B. The impedance spectra together with the rate data in Fig. 6 and 7 strongly suggest that low cell impedances resulting from an optimized composition as well as proper processing of the cathode are necessary to obtain high utilizations in $Li_4Ti_5O_{12}$//solid polymer electrolyte/$LiMn_2O_4$ full cells at rates over 1C. Judging from these observations, a total impedance of $\leq$40 Ω cm^2 can be considered as the signature of a full cell capable of performing well at high rates.

It is also of significant interest to examine the behavior of the cell on charge. The latter is not addressed in most investigations. However, from the point of view of some applications, e.g., portable electronics, rapid charging may be just as important as high rate discharging. In general, for a lithium-ion cell such as this $Li_4Ti_5O_{12}$//solid polymer electrolyte//$LiMn_2O_4$ system, there is no possibility of Li plating during a high rate charge and, as a result, one would expect the charge behavior to be similar to the discharge behavior. This charge/discharge symmetry can be broken, however, because the charge voltage plateau of the $LiMn_2O_4$ electrode is located close to the cutoff potential and any significant polarization of this electrode during charge forces the cell to reach the cutoff prematurely leading to a significant loss of utilization. During high rate discharge, however, electrode polarization is in the opposite direction and the system is able to handle a far higher electrode polarization without any significant effect on utilization.

Figures 9 and 10 compare the effect of charge rate on the capacity for cells A (Fig. 6) and B (Fig. 7). The rate of charge was increased as indicated on each figure in milliamperes per centimeter squared and the discharge was performed at a low rate, 0.02 mA/cm^{-2} (~C/30). For cell B the symmetry in the discharge (Fig. 7) and charge processes (Fig. 10) appears to have been preserved up to a rate of 1C (0.6 mA/cm^2). At higher charge rates, capacity utilization on charge appears to be seriously lagging behind that for the corresponding discharge. Again, cell B with lower impedance performs better.

Discussion on the effect of charge rate on the capacity utilization can be further highlighted by examining the evolution of individual electrode potentials during charge. Such information are presented in Fig. 11 for cell A and in Fig. 12 for cell B. The cathode used in cell A with the higher total impedance appears to undergo significant polarization at high rates leading to a rapid loss of capacity. The anode appears to be behaving well, partly due to its under utilization related to polarization of the cathode. In contrast, the cathode in cell B appears to undergo minimal polarization and the imposition of the cutoff potential now comes from the anode polarization.

The results presented clearly show that achieving low impedance for the cathode is the key for full cells to yield high utilization at high charge and discharge rates.

Pulsing capability of $Li_4Ti_5O_{12}$//solid polymer electrolyte//$LiMn_2O_4$ cells.—Pulsing capability of a battery becomes an important issue in applications where battery power is delivered as high rate pulses of brief duration, e.g.,

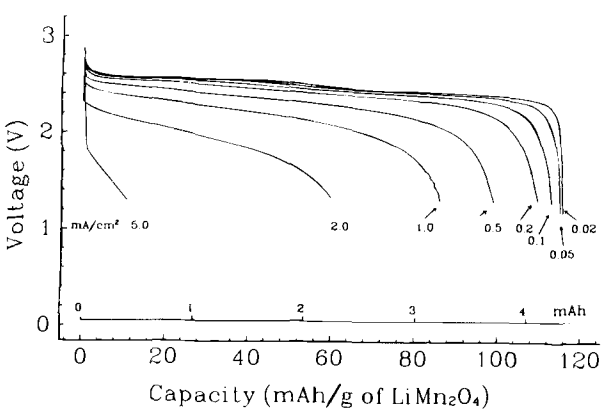

Fig. 6. The voltage vs. capacity profiles at ambient temperature for the capacity balanced $Li_4Ti_5O_{12}$//solid polymer electrolyte//$LiMn_2O_4$ cell A as a function of different discharge rates. The cathode had 4.4 mAh capacity, 10 cm^2 (2.5 × 4.0 cm) active area, and a thickness of 43 μm. The anode had a 4.5 mAh capacity, 11.3 cm^2 (2.7 × 4.2 cm) active area, and a thickness of 28 μm. The solid polymer electrolyte thickness was 88 μm. Current densities are indicated.

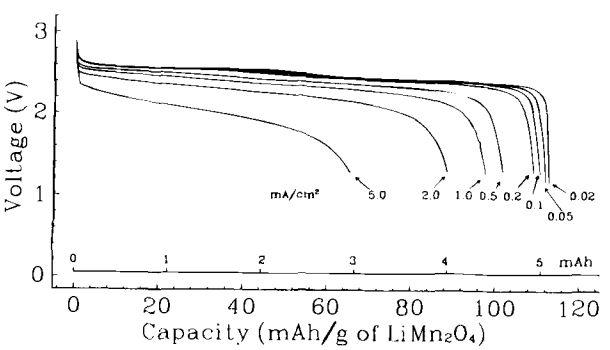

Fig. 7. The voltage vs. capacity profiles at ambient temperature for the capacity balanced $Li_4Ti_5O_{12}$//solid polymer electrolyte//$LiMn_2O_4$ cell B as a function of different discharge rates. The cathode has a 5.4 mAh capacity, 10 cm^2 (2.5 × 4.0 cm) active area, and a thickness of 45 μm. The anode had 5.3 mAh capacity, 11.3 cm^2 (2.7 × 4.2 cm) active area, and a thickness of 28 μm. The solid polymer electrolyte thickness was 88 μm. Current densities are as indicated.

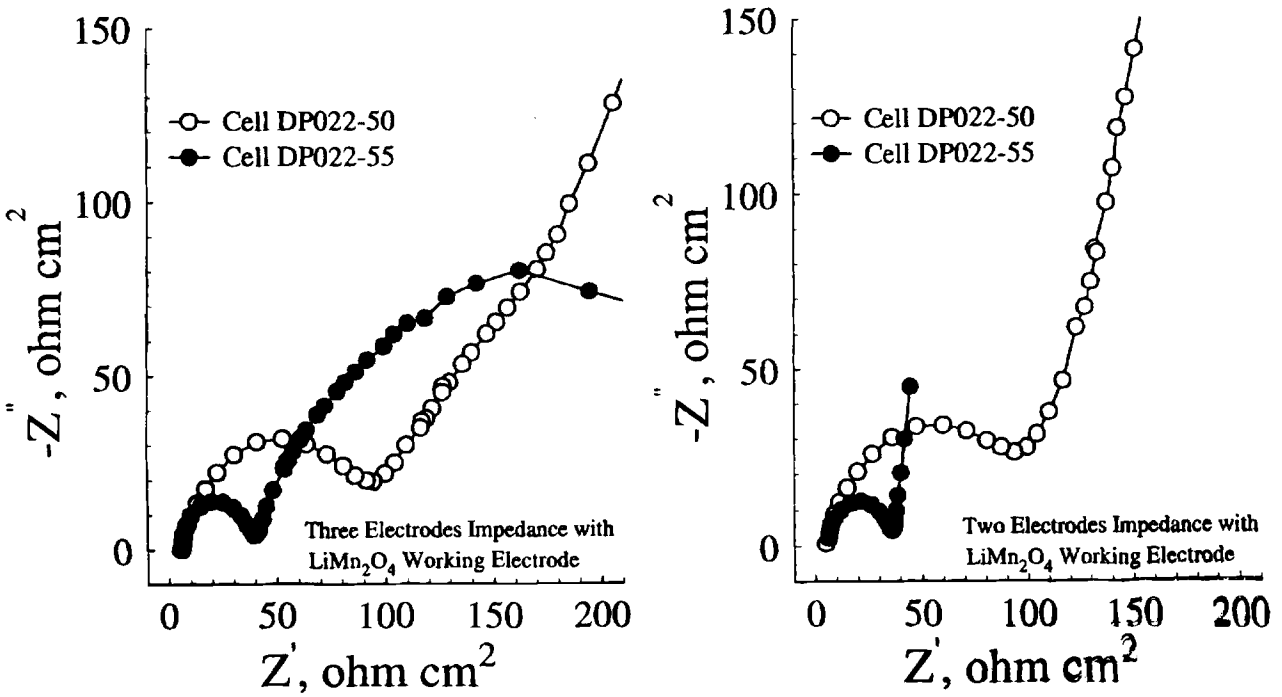

Fig. 8. Impedance spectra of cells A (DP022-50) and B (DP022-55) at cycle 2. (a, left) Impedance measured in three-electrode configuration with $LiMn_2O_4$ as the working electrode. An ac modulation of 5 mV was applied across the cell under open-circuit condition in the frequency range of 0.1 Hz to 100 kHz. (b, right) Impedance measured as in Fig. 8a except in two-electrode configuration with $LiMn_2O_4$ as the working electrode.

cranking of an automobile and transmission of digital data in a personal communication system. The pulse discharge capability of the $Li_4Ti_5O_{12}$//solid polymer electrolyte// $LiMn_2O_4$ cells were studied. A cell was charged to 2.9 V at 0.02 mA/cm^2 before pulse discharging to 1.2 V at current densities of 5, 7.5, and 10 mA/cm^2, corresponding to rates between 20 C and 16 C. A pulse width of 10 ms and an interpulse relaxation time of 50 ms were used. Figures 13 and 14, respectively, show the evolution of ON voltage and OFF voltage during the 10 mA/cm^2 pulse discharge, and the voltage vs. time profile of two pulses, chosen arbitrarily. The initial drop in voltage at the onset of a pulse corresponds to the ohmic voltage drop due to the total cell resistance. The results from pulse discharge tests are presented in Table II.

Resistance calculated from individual pulse data appeared to be on the same order of magnitude as the total impedance (R_b plus R_{ct} in Fig. 3) determined from the impedance measurement. Resistance obtained from the pulse data appears to be slightly higher than that obtained from impedance because the initial drop occurring at the onset of a pulse may also involve Helmholtz potential drops resulting from charging of interfaces. The utilization observed for the same cell during a continuous discharge at 5 mA/cm^2 was close to 50 mAh/g of $LiMn_2O_4$. In contract, discharge in the pulse mode at the same rate yielded nearly twice as much capacity. The increased efficiency in utilization may be the result of having a long rest period after a current pulse which allows Li to migrate from the surface to the bulk of the active particle, prior to the next pulse.

The energy density of the $Li_4Ti_5O_{12}$//PAN-electrolyte// $LiMn_2O_4$ cell, calculated using a cell voltage of 2.6 V and the cathode and anode capacities observed at the C/10 discharge, is 60 Wh/kg. The weights of cathode, anode, electrolyte, and current collector are included in this calculation.

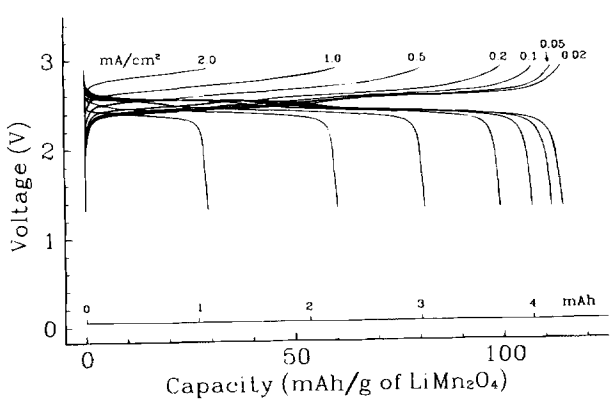

Fig. 9. Comparison of the voltage vs. capacity profiles at various rates for $Li_4Ti_5O_{12}$//solid polymer electrolyte//$LiMn_2O_4$ cell A (Fig. 6). Charge currents are indicated. Discharge current was constant at 0.02 mA/cm^2. Cycling started with a charge at 0.02 mA/cm^2.

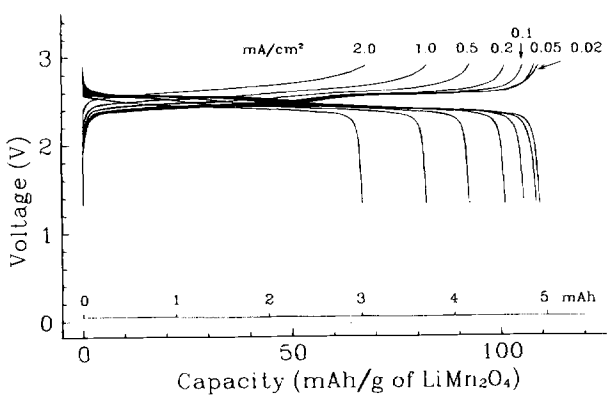

Fig. 10. Comparison of the voltage vs. capacity profiles on individual electrodes at various charge rates for $Li_4Ti_5O_{12}$//solid polymer electrolyte//$LiMn_2O_4$ cell B (Fig. 7). Charge currents are indicated in the figure. Discharge current was constant at 0.02 mA/cm^2. Cycling started with a charge at 0.02 mA/cm^2.

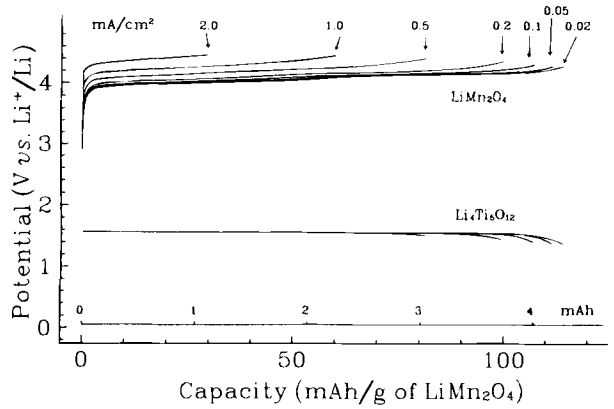

Fig. 11. Comparison of the voltage vs. capacity profiles of individual electrodes at various charge rates for Li_4Ti5O_{12}//solid polymer electrolyte//$LiMn_2O_4$ cell A. Charge currents are indicated. Discharge current was constant at 0.02 mA/cm².

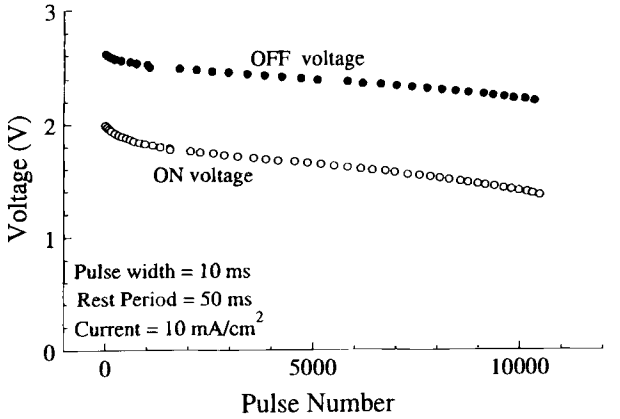

Fig. 13. Pulse discharge data of a $Li_4Ti_5O_{12}$//solid polymer electrolyte//$LiMn_2O_4$ cell at 10 mA/cm² at changes in the cell voltage during the course of pulsing expressed as ON voltage and OFF voltage as a function of the total number of pulses.

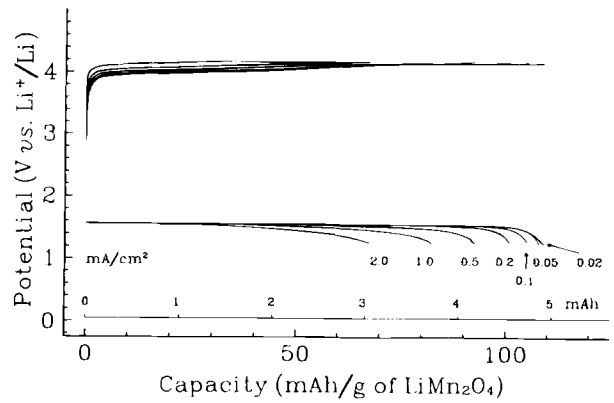

Fig. 12. Comparison of the voltage vs. capacity profiles of individual electrodes at various charge rates for $Li_4Ti_5O_{12}$// solid polymer electrolyte//$LiMn_2O_4$ cell B. Charge currents are indicated. Discharge current was constant at 0.02 mA/cm².

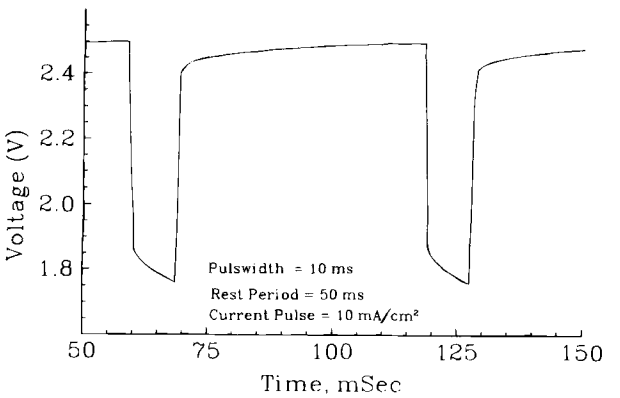

Fig. 14. Voltage profiles of two pulses chosen arbitrarily.

Table II. Summary of results from pulse discharge experiments.

Current pulse (mA/cm²)	C rate (C)	Total No. of pulses	Total capacity (mAh)	Capacity (mAh/g) of $LiMn_2O_4$	Capacity (mAh/g) of $Li_4Ti_5O_{12}$	Initialload voltage (V)	Ohmic voltge drop at pulse onset (V)	Calculated cell resistance (Ω)	Total cell impedance from EIS (Ω)
5.0	8	31,000	4.3	103.2	136.5	2.62	0.32	6.4	4.2
7.5	12	18,600	3.9	93.6	123.8	2.18	0.51	6.8	3.9
10.0	16	10,500	2.9	69.6	92.1	2.02	0.65	6.5	4.0

Acknowledgment

This work was carried out on contract DE-FG02-96ER82158 from the U.S Department of Energy.

Manuscript submitted August 21, 1997; revised manuscript received March 19, 1998.

REFERENCES

1. R. LaFollete and D. Bennion, *J. Electrochem. Soc.*, **137**, 3693 (1990).
2. S. Atlung, K. West, and T. Jacobsen, *J. Electrochem. Soc.*, **126**, 1311 (1979).
3. J. Newman, *J. Electrochem. Soc.*, **142**, 97 (1995).
4. M. Doyle, J. Newman, A. S. Gozdz, C. N. Schmutz, and J. M. Tarascon, *J. Electrochem. Soc.*, **143**, 1890 (1996).
5. E. Peled, *J. Electrochem. Soc.*, **126**, 2047 (1979).
6. J. G. Thevenin and R. H. Muller, *J. Electrochem. Soc.*, **134**, 273 (1987).
7. D. Aurbach, Y. Gofer, M. Ben-Zion, and P. Aped, *J. Electroanal. Chem.*, **339**, 451 (1992).
8. D. Aurbach, Y. E. Eli, O. Chusid, Y. Carmeli, M. Babai, and H. Yamin, *J. Electrochem. Soc.*, **141**, 603 (1994).
9. R. Fong, U. von Sacken, and J. R. Dahn, *J. Electrochem. Soc.*, **137**, 2009 (1990).
10. Z. Jiang, M. Alamgir, and K. M. Abraham, *J. Electrochem. Soc.*, **142**, 333 (1995).
11. A. N. Dey and B. P. Sullivan, *J. Electrochem. Soc.*, **117**, 295 (1970).
12. D. Peramunage and K. M. Abraham, *J. Electrochem. Soc.*, **145**, 2609 (1998).
13. T. Ohzuku, A. Ueda, and N. Yamamoto, *J. Electrochem. Soc.*, **137**, 769 (1990).
14. E. Ferg, R. J. Gummow, A. de Kock, and M. M. Thackeray, *J. Electrochem. Soc.*, **141**, L147 (1994).
15. H. S. Choe, B. G. Carroll, D. M. Pasquariello, and K. M. Abraham, *J. Electrochem. Soc.*, **9**, 369 (1997).
16. J. G. Thevenin and R. H. Muller, *J. Electrochem. Soc.*, **134**, 273 (1987).
17. N. Takami, T. Ohsaki, and K. Inada, *J. Electrochem. Soc.*, **139**, 1849 (1992).
18. S. Morzilli, F. Bonino, and B. Scrosati, *Electrochim. Acta*, **32**, 961 (1987).

19. M. G. S. R. Thomas, P. G. Bruce, and J. B. Goodenough, *J. Electrochem. Soc.*, **132**, 1521 (1985).
20. C. Ho, I. D. Raistrick, and R. A. Huggins, *J. Electrochem. Soc.*, **127**, 343 (1980).
21. D. Guyomard and J. M. Tarascon, *J. Electrochem. Soc.*, **139**, 937 (1992).
22. D. Guyomard and J. M. Tarascon, *J. Electrochem. Soc.*, **140**, 3071 (1993).

Metastable Pitting and the Critical Pitting Temperature

N. J. Laycock,*,[a] M. H. Moayed,[b] and R. C. Newman,[b]**

[a]*Gracefield Research Center, Materials Performance Technologies, Lower Hutt, New Zealand*
[b]*University of Manchester Institute of Science and Technology, Corrosion and Protection Center, Manchester M60 1QD, England*

ABSTRACT

For any particular stainless steel, a critical pitting temperature (CPT) can be measured, below which stable pits do not occur at any potential up to the onset of transpassivity. The more highly alloyed the steel, particularly with molybdenum, the higher the CPT. The CPT for 904L austenitic stainless steel with a 240 grit surface finish has been determined as 48 to 49°C, and metastable pitting events have been analyzed in detail at lower temperatures. Below the CPT, metastable pitting activity peaks at around 300 mV (SCE), but occurs at all potentials up to the transpassive range. The morphology of these pits has been examined using SEM and a model is proposed in which precipitation of an anodic salt film within pits is the critical factor; above the CPT, a salt film is essential for stable pit growth, while below the CPT, the salt is an intermediary in oxide passivation, like that of iron in sulfuric acid. This is an outcome of a complex dynamical system and does not require the properties of the salt itself to change suddenly with temperature.

Introduction

The pitting potential of stainless steels shows a discontinuous variation with temperature. The critical pitting temperature (CPT) for a given alloy and surface finish is defined as the temperature below which no stable pitting can occur, and is indicated by a step decrease of the breakdown potential with increasing temperature, from a value in the transpassive range to a moderate value representing a true pitting potential. The concept of a CPT was introduced by Brigham and Tozer[1-3] as a means of screening austenitic stainless steels of differing molybdenum content. Qvarfort[4] demonstrated independence of the CPT on chloride concentration in the range 1 to 5 M NaCl, and also found it to be independent of pH in the range 1 to 7. Qvarfort's results also indicate that the CPT represents a very sharp transition and, in the absence of unwanted crevice corrosion, it can be defined within an absolute accuracy of ~1°C. Obviously the CPT results from some deterministic process. It does, however, depend on the geometry of possible pit initiation sites; recently we have found[5] that the CPT varies appreciably with surface finish.

It was found[2,3] that molybdenum content was the most important factor in determining the CPT of a given alloy but the effect of other elements can also be included to produce an empirical pitting resistance equivalent (PRE). Different authors[6-8] have quoted different equations for the PRE (e.g., Eq. 1), but the CPT in all cases increases linearly with increasing PRE

$$\text{PRE} = \text{Cr (wt \%)} + 3.3\ \text{Mo (wt \%)} + 30\ \text{N (wt \%)} \quad [1]$$

The CPT is a transition related to early growth of stable pits. Propagation of stable pits, or initiation of metastable pits, may occur at lower temperatures. In order to understand the CPT, we must recognize that the driving force for metal dissolution is enormous at high anodic potentials such as 750 mV (SCE) where CPT tests are commonly carried out. It is unlikely that alloying could ennoble the steel enough to prevent the establishment of a concentrated pit chemistry by rapid metal dissolution at this potential. The mechanism of the CPT transition must therefore involve passivation, not ennoblement, and this is the hypothesis on which we have based our recent work in this area.

In order to gain a microscopic understanding of the CPT, one first hopes to find a similar transition that occurs on larger electrodes and in a deterministic manner. Newman and Liew[9] used artificial pit electrodes of stainless steels and high nickel alloys to measure repassivation temperatures for localized corrosion. They found that propagation of deep pits held at high anodic potentials was possible at temperatures well below the CPT, but on cooling, these pits repassivated abruptly under their anodically generated salt films at a lower critical temperature T_r. It was suggested that smaller pits would have repassivated nearer the CPT. Later, Salinas-Bravo and Newman[10] used electrochemical noise from duplex stainless steel to show that metastable pitting could occur at temperatures below the CPT, but stable pitting was only detected at the conventional CPT value. This suggested that the CPT was related to the transition from metastable to stable pit growth, and they suggested the following explanation. Assume all stable pits must develop and maintain an anodic salt film. Assume further that there is a critical current density for passivation in the saturated salt environment of the pit nucleus, i_{crit}, which increases with temperature, T. There is also a limiting current density, i_{lim}, given by the saturation concentration of metal ions, C_{sat}, and Fick's first law, which increases more gradually with T than i_{crit}. The CPT corresponds to the temperature at which $i_{crit} \approx i_{lim}$, since below this temperature the alloy cannot generate the anodic current density required to maintain the necessary pit chemistry. The present paper combines some ideas from the work of Liew[9] and Salinas-Bravo,[10] granting the salt film a causal role in passivation as suggested by Liew, but considering also the balance between dissolution and mass transport in a small cavity.

Experimental

All electrochemical experiments used a potentiostat made by ACM Research together with a sweep generator made by Thompson Instruments. Data were recorded digitally by a computer fitted with a Keithley Instruments data acquisition card used as an analog to digital converter, in conjunction with Keithley Easyest LX software. A saturated calomel (SCE) or silver/silver chloride (Ag/AgCl) electrode was used as the reference electrode, and a 10 mm length of 1 mm diam platinum wire as the counter electrode. All test solutions were made from analytical grade chemicals and deionized water.

The work was performed on 904L stainless steel plate (20 Cr, 25 Ni, 4.3 Mo, 1.5 Cu, 1.4 Mn, < 0.003 S), machined into 4.5 mm diam rod specimens. The steel was supplied by

* Electrochemical Society Student Member.
** Electrochemical Society Active Member.